Quantum Simulation with Gauge Fixing: from Ising Lattice Gauge Theory to Dynamical Flux Model

Junsen Wang,[1, 2, *] Xiangxiang Sun,[3, 4] and Wei Zheng[3, 4, 5, †]

[1]*Center of Materials Science and Optoelectronics Engineering,*
College of Materials Science and Opto-electronic Technology,
University of Chinese Academy of Sciences, Beijing 100049, China
[2]*CAS Key Laboratory of Theoretical Physics, Institute of Theoretical Physics, Chinese Academy of Sciences, Beijing 100190, China*
[3]*Hefei National Research Center for Physical Sciences at the Microscale and School of Physical Sciences,*
University of Science and Technology of China, Hefei 230026, China
[4]*CAS Center for Excellence in Quantum Information and Quantum Physics,*
University of Science and Technology of China, Hefei 230026, China
[5]*Hefei National Laboratory, University of Science and Technology of China, Hefei 230088, China*
(Dated: July 2, 2024)

Quantum simulation of synthetic dynamic gauge field has attracted much attentions in recent years. There are two traditional ways to simulate gauge theories. One is to directly simulate the full Hamiltonian of gauge theories with local gauge symmetries. And the other is to engineer the projected Hamiltonian in one gauge subsector. In this work, we provide the third way towards the simulation of gauge theories based on *gauge fixing*. To demonstrate this concept, we fix the gauge of an Ising lattice gauge field coupled with spinless fermions on a ladder geometry. After the gauge fixing, this gauge theory is reduced to a simpler model, in which fermions hop on a ladder with a fluctuating dynamical $\mathbb{Z}_2$ flux. Then we shows that this model can be realized via Floquet engineering in ultracold atomic gases. By analytical and numerical studies of this dynamical flux model, we deduce that there is confinement to deconfinement phase transition in the original unfixed gauge theory. This work paves the way to quantum simulate lattice gauge theory using the concept of gauge fixing, relevant both for condensed matter and high energy physics.

I. INTRODUCTION

Lattice gauge theories (LGTs) have both fundamental and practical importance in modern physic [1–3]. It is originally proposed by Wilson as a non-perturbative framework to deal with quantum chromodynamics (QCD) in the strong coupling region [4]. Soon after, in combination with Monte-Carlo methods, it becomes a standard numerical approach to QCD. LGT can also emerge from strongly correlated quantum materials, such as quantum spin liquids [5] and high T_c superconductors [6]. More recently, the concept of LGT has extended to the territory of quantum computation and information. For example, the celebrated toric code model is essentially a $\mathbb{Z}_2$ LGT. However due to the massive local constraints imposed by the gauge symmetry and the limitation of classical computers, it is challenging to study the real-time dynamics of LGTs.

In the last decade, quantum simulation based on artificial quantum systems, such as ultracold atoms [7–11], trapped ions [12, 13], Rydberg atoms in optical tweezers [14, 15], and superconducting circuits [16–22], gradually evolves as a refreshing tool to attack this hard problem [23–51]. Up to now there are two main routes to quantum simulate LGT. The first is to directly simulate the full Hamiltonian of LGT with massive local gauge symmetries. For example, in 2019, a $\mathbb{Z}_2$ LGT has been realized via Floquet engineering in a double well [52]. In 2020, a quantum link model, one particular U(1) LGT, has been simulated up to 71 sites in an optical

lattice [53]. In the same year, U(1) LGT has also been realized in atomic mixture [54]. The second route is to simulate the Hamiltonian in one gauge sector. In this situation, the local gauge symmetry can emerge from the local constraints. For instance, the Rydberg blockade effect has been used to simulate the quantum link model in the gauge invariant subsector [14, 15]. These progresses have motivated extensive studies in the two directions.

In this work, we propose *gauge fixing* as the third route towards quantum simulation of LGTs. In fact, gauge fixing has been widely used to deal with gauge theories defined in continuous space-time. For example in electromagnetism, one can fix the gauge by choosing the Coulomb, Lorenz or Landau gauge in practical calculations. Though gauge fixing is not obligatory in LGTs, it has been implemented in the context of Monte-Carlo computation of LGTs [55]. However, gauge fixing is much less explored in the modern era of quantum simulation on the Hamiltonian level. Compare to the usual Faddeev-Popov-De Witt gauge fixing procedure based on path integral [56, 57], we clarify the concept of gauge fixing on the Hamiltonian level. The proper gauge fixing procedure require that the matrix elements of both the Hamiltonian and gauge invariant observables to be unchanged. After gauge fixing, the rigorous requirement of local gauge invariance is bypassed, and the Hilbert space is significantly reduced. The fixed Hamiltonian becomes much simpler and relatively easy to implement in experiment.

To illustrate the gauge fixing procedure, we fix the gauge of an Ising LGT coupled with fermions on a ladder geometry. After gauge fixing, the Hamiltonian is largely simplified, and describes fermions hopping on a ladder subject to a fluctuating dynamical flux. We then propose a Floquet engi-

---
* jsw@ucas.ac.cn
† zw8796@ustc.edu.cn

neering scheme to simulate this gauge-fixed Hamiltonian. We used two species ultracold fermions on a ladder optical lattice. One is to simulate the gauge field, and the other to simulate the matter field. The zero temperature phase diagram of this fixed model is determined via analysis in the limiting cases and the numerical density-matrix renormalization group (DMRG) calculation. We note that this model basically exhibit two phases. One is antiferromagnetic Néel order phase, and the other is the paramagnetic phase, which are reminiscent of the confinement and deconfinement phases in the original unfixed model.

This paper is organized as follows. In the next section, we first clarify the concept of gauge fixing on the Hamiltonian level. Then in Sec. III, we fix the gauge of an Ising LGT coupled with fermions on a ladder geometry. We then propose a Floquet engineering scheme to simulate this gauge-fixed Hamiltonian in Sec. IV. Next the ground state of this model is determined via analysis in the limiting cases and the numerical density-matrix renormalization group (DMRG) calculation, in Sec. V and VI, respectively. Lastly, we give a discussion and outlook in Sec. VII.

II. GAUGE FIXING ON THE HAMILTONIAN LEVEL

Gauge fixing is crucial for gauge theories in continuous space-time. The Feynman integral of the historical paths connected by gauge transformation will give a divergent propagator. Thus in continuous space-time, one has to choose a particular gauge to eliminate the redundancy of gauge transformation.

In LGTs, gauge fixing is not essential. However, just as discussed in introduction, gauge fixing can largely reduce the Hilbert space, thus can effectively simplify the experiments for simulations. In the following we will first introduce the concept of gauge fixing on the Hamiltonian level.

Given a Hamiltonian of a LGT, H. It processes local gauge symmetry as $[G_i, H] = 0$, where G_i is the local gauge transformation operator defined on each site. As a result, G_i and H share the eigen states,

$$H |\psi\rangle = E |\psi\rangle, \tag{1}$$
$$G_i |\psi\rangle = g_i |\psi\rangle. \tag{2}$$

According to g_i, the eigen values of G_i, the Hamiltonian can be block diagonalized into disconnected gauge sectors,

$$H = \begin{bmatrix} \ddots & & & \\ & H_{\{g_i'\}} & & \\ & & H_{\{g_i\}} & \\ & & & \ddots \end{bmatrix}. \tag{3}$$

Here $H_{\{g_i\}}$ is the Hamiltonian inside each gauge sector.

Usually people are interesting in the so-called *physical sector* or the *gauge invariant sector*, in which $g_i = 1$ for all site. Thus all states in this sector are gauge invariant, $G_i |\psi_{\text{GI}}\rangle = |\psi_{\text{GI}}\rangle$.

All orthogonal wave functions can be classified into different gauge classes,

$$C^{[1]} = \left(\left| \psi_1^{[1]} \right\rangle, \left| \psi_2^{[1]} \right\rangle, \cdots, \left| \psi_V^{[1]} \right\rangle \right), \tag{4}$$
$$C^{[2]} = \left(\left| \psi_1^{[2]} \right\rangle, \left| \psi_2^{[2]} \right\rangle, \cdots, \left| \psi_V^{[2]} \right\rangle \right), \tag{5}$$
$$\vdots \tag{6}$$
$$C^{[D]} = \left(\left| \psi_1^{[D]} \right\rangle, \left| \psi_2^{[D]} \right\rangle, \cdots, \left| \psi_V^{[D]} \right\rangle \right), \tag{7}$$

Here V is the number of total independent gauge transformations, and D is the number of gauge classes. Wave functions belong to the same gauge class are related by a gauge transformation, $\left| \psi_\alpha^{[k]} \right\rangle = G \left| \psi_\beta^{[k]} \right\rangle$. The wave functions belong to different gauge classes can not be transformed into each other by any gauge transformations.

The basis of the gauge invariant sector can be constructed by these gauge classes via equal-weight superposition of all the wave functions inside one gauge class,

$$\left| \psi_{\text{GI}}^{[k]} \right\rangle = \frac{1}{\sqrt{V}} \sum_{\alpha=1}^{V} \left| \psi_\alpha^{[k]} \right\rangle. \tag{8}$$

Such superposition is gauge invariant, since any gauge transformation is just a rearrangement of the summation. The gauge fixing on the Hamiltonian level is freezing some degree of freedoms of the gauge field. The goal of the freezing is to pick up one particular wave function in each gauge class,

$$C^{[1]} \xrightarrow{\text{gauge fixing}} \left| \psi_\alpha^{[1]} \right\rangle, \tag{9}$$
$$C^{[2]} \xrightarrow{\text{gauge fixing}} \left| \psi_\beta^{[2]} \right\rangle, \tag{10}$$
$$\vdots \tag{11}$$
$$C^{[D]} \xrightarrow{\text{gauge fixing}} \left| \psi_\gamma^{[D]} \right\rangle, \tag{12}$$

After this gauge fixing the dimension of the Hilbert space is suppressed to D, and the gauge transformations can not be applied. At the same time, the gauge fixing rule is also applied on the Hamiltonian and gauge invariant observables,

$$H \xrightarrow{\text{gauge fixing}} H_{\text{fixed}}, \tag{13}$$
$$O \xrightarrow{\text{gauge fixing}} O_{\text{fixed}}, \tag{14}$$

We require the gauge fixing rule to ensure that

$$\left\langle \psi_{\text{GI}}^{[q]} \right| H \left| \psi_{\text{GI}}^{[p]} \right\rangle = \left\langle \psi_\alpha^{[q]} \right| H_{\text{fixed}} \left| \psi_\beta^{[p]} \right\rangle, \tag{15}$$
$$\left\langle \psi_{\text{GI}}^{[q]} \right| O \left| \psi_{\text{GI}}^{[p]} \right\rangle = \left\langle \psi_\alpha^{[q]} \right| O_{\text{fixed}} \left| \psi_\beta^{[p]} \right\rangle. \tag{16}$$

Note that after the gauge fixing, one faithfully reconstruct the matrix elements of Hamiltonian in the gauge invariant sector.

If one want to calculate the eigen states in the gauge invariant sector, we can first compute the eigen states of H_{fixed} as

$$|\psi\rangle = \sum_{q=1}^{D} a_q \left| \psi_\alpha^{[q]} \right\rangle, \tag{17}$$
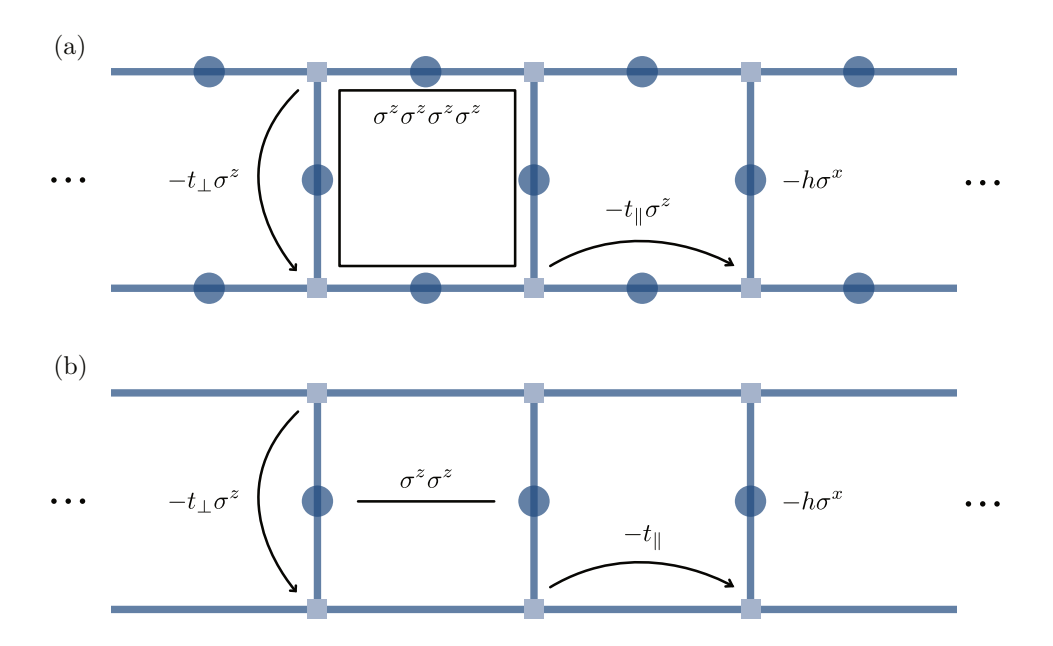
FIG. 1. (a) Schematic of the gauge invariant Hamiltonian, Eq. (21). Spinless fermions live on the vertices and Ising spins live on the legs and rungs. (b) Schematic of the gauge invariant Hamiltonian *after gauge fixing*, Eq. (34). Note that the Ising spins now only live on the rungs.

Then the corresponding gauge invariant eigen state can be expressed as

$$|\psi_{\text{GI}}\rangle = \frac{1}{\sqrt{V}} \sum_{\beta=1}^{V} G_\beta |\psi\rangle \qquad (18)$$

$$= \sum_{q=1}^{D} a_q \frac{1}{\sqrt{V}} \sum_{\beta=1}^{V} G_\beta \left|\psi_\alpha^{[q]}\right\rangle \qquad (19)$$

$$= \sum_{q=1}^{D} a_q \left|\psi_{\text{GI}}^{[q]}\right\rangle, \qquad (20)$$

where G_α are all possible independent gauge transformations. In the gauge fixing process, some degree of freedoms are frozen. We have to unfreeze them when reconstructing the gauge invariant wave functions, such that the gauge transformation can be applied.

III. GAUGE FIXING FOR AN ISING LATTICE GAUGE FIELD COUPLED WITH FERMIONS ON A LADDER

The gauge invariant Hamiltonian of an Ising lattice gauge field coupled with spinless fermions, on which we focus in

this work, is defined on a ladder geometry [see Fig. 1(a)],

$$H = -t_\perp \sum_j \left(c_{jL}^\dagger \sigma_j^z c_{jR} + \text{H.c.}\right)$$
$$- t_\parallel \sum_{j\alpha} \left(c_{j\alpha}^\dagger \sigma_{\langle j,j+1\rangle\alpha}^z c_{j+1,\alpha} + \text{H.c.}\right)$$
$$+ U_1 \sum_j \sigma_j^z \sigma_{\langle j,j+1\rangle,R}^z \sigma_{j+1}^z \sigma_{\langle j,j+1\rangle,L}^z - h \sum_j \sigma_j^x, \qquad (21)$$

Here, the first two lines describe fermions hopping along the longitudinal (leg) and transverse (rung) directions interacting with the Ising gauge fields according to the minimal coupling procedure. And $\sigma_{\alpha\langle j,j+1\rangle}^z$ denotes the Ising gauge field sitting on the $\alpha = L, R$ leg between site j and site $j+1$. The last line is the $\mathbb{Z}_2$ analog of magnetic field and electric field energy, respectively. Comparing to the standard Ising LGT, here the electric field term only exists on the rungs.

The Hamiltonian Eq. (21) has local Ising gauge symmetries. The corresponding gauge transformation operator is

$$G_{j\alpha} = e^{i\pi n_{j\alpha}} \sigma_{\langle j-1,j\rangle,\alpha}^x \sigma_j^x \sigma_{\langle j,j+1\rangle,\alpha}^x, \qquad (22)$$

where $n_{j\alpha} = c_{j\alpha}^\dagger c_{j\alpha}$. It commutes with the Hamiltonian,

$$[G_{j\alpha}, H] = 0, \qquad (23)$$

As we discussed in the previous section, in gauge invariant sector, $G_{j\alpha} = 1$ on all site. As a result, in this sector we have

$$e^{i\pi n_{j\alpha}} = \sigma_{\langle j-1,j\rangle,\alpha}^x \sigma_j^x \sigma_{\langle j,j+1\rangle,\alpha}^x. \qquad (24)$$

This is nothing but the $\mathbb{Z}_2$ version of Gauss' law, which imposes extensive local constrains on the dynamics of the system.
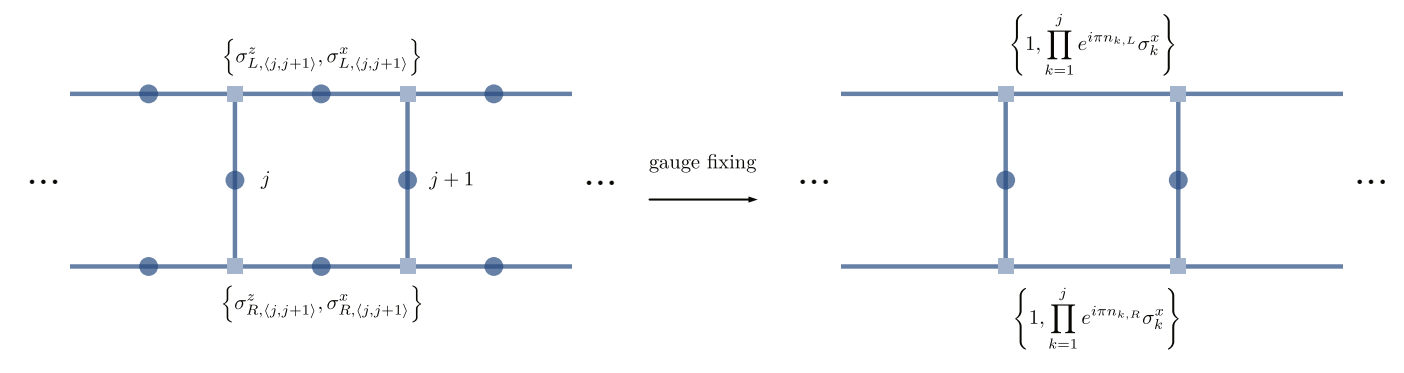
FIG. 2. Gauge fixing for an Ising lattice gauge field coupled with fermions on a ladder. Before the gauge fixing, shown in the left, there is a spin-1/2 (fermionic) degree of freedom on each link (site), denoted by a blue dot (square). After gauge fixing, shown in the right, local Hilbert spaces on the links of two legs are eliminated, indicated by the absence of blue dots and the replacement of the corresponding operators there. One can consecutively fix the gauge for two legs starting from the leftmost side.

In a gauge theory, only the gauge invariant observable has non-vanishing expectation values. In our model there are two common gauge invariant observables. One is the Wilson loop,

$$W(i,j) = \left\langle \sigma_i^z \left(\prod_{k=i}^{j-1} \sigma_{\langle k,k+1\rangle,L}^z \sigma_{\langle k,k+1\rangle,R}^z \right) \sigma_j^z \right\rangle, \quad (25)$$

which can be used to diagnose confinement or deconfinement phases. The other is the gauge invariant correlations of fermions,

$$C_{\alpha\alpha}(i,j) = \left\langle c_{i\alpha} \left(\prod_{\text{string}} \sigma^z \right) c_{j\alpha}^\dagger \right\rangle, \quad (26)$$

where the string connects the two fermion sites

Now we are going to fix the gauge of this model. A typical basis of this Ising Lattice gauge model is

$$|\psi\rangle = |\varphi\rangle_{\text{fermi}}$$
$$\otimes \left| \xi_1, \xi_2, \cdots ; \xi_{\langle 1,2\rangle,L}, \xi_{\langle 2,3\rangle,L}, \cdots ; \xi_{\langle 1,2\rangle,R}, \xi_{\langle 2,3\rangle,R}, \cdots \right\rangle, \quad (27)$$

where $\xi = \uparrow, \downarrow$ is the states of the gauge field on the link. Then one can perform the gauge fixing process by freezing the gauge field degree of freedom on the legs as

$$|\psi\rangle \xrightarrow{\text{gauge fixing}} |\varphi\rangle_{\text{fermi}} \otimes |\xi_1, \xi_2, \cdots ; \uparrow, \uparrow, \cdots ; \uparrow, \uparrow, \cdots\rangle, \quad (28)$$

Then the gauge fixing of the spin operator on the legs corresponds to

$$\sigma_{\langle i,j+1\rangle,\alpha}^z \xrightarrow{\text{gauge fixing}} 1, \quad (29)$$

Since $\sigma_{\langle j,j+1\rangle,\alpha}^x$ on the legs can flip the flux of the corresponding plaquette, it can not be simply replaced by a c-number. Instead, one can use the Gauss' law to replace it by other spin operators as

$$\sigma_{\langle j,j+1\rangle,\alpha}^x = e^{i\pi\hat{n}_{j\alpha}} \sigma_{\langle j-1,j\rangle,\alpha}^x \sigma_j^x, \quad (30)$$

Moreover, $\sigma_{\langle j-1,j\rangle,\alpha}^x$ should also be fixed. Thus we can obtain

$$\sigma_{\langle j,j+1\rangle,\alpha}^x = \prod_{k=1}^{j} e^{i\pi\hat{n}_{k\alpha}} \sigma_k^x, \quad (31)$$

Note that it becomes a highly non-local operators. So our gauge fixing rules for the spin operators on legs are summarized as

$$\sigma_{\langle j,j+1\rangle,\alpha}^z \xrightarrow{\text{gauge fixing}} 1, \quad (32)$$

$$\sigma_{\langle j,j+1\rangle,\alpha}^x \xrightarrow{\text{gauge fixing}} \prod_{k=1}^{j} e^{i\pi\hat{n}_{k\alpha}} \sigma_k^x \quad (33)$$

After this gauge fixing process, the Hamiltonian becomes [see Fig. 1(b)]

$$\begin{aligned} H_{\text{fixed}} &= -t_\perp \sum_j \left(c_{jL}^\dagger \sigma_j^z c_{jR} + \text{H.c.} \right) \\ &\quad -t_\parallel \sum_{j\alpha} \left(c_{j\alpha}^\dagger c_{j+1,\alpha} + \text{H.c.} \right) \\ &\quad +U_1 \sum_j \sigma_j^z \sigma_{j+1}^z - h \sum_j \sigma_j^x, \quad (34) \end{aligned}$$

Note that in our simple model, there is no electric field term on the legs. Therefore after gauge fixing the Hamiltonian is still local. The Wilson loop and fermion correlation becomes

$$W_\Gamma(i,j) \xrightarrow{\text{gauge fixing}} \left\langle \sigma_i^z \sigma_j^z \right\rangle, \quad (35)$$

$$C_{\alpha\alpha}(i,j) \xrightarrow{\text{gauge fixing}} \left\langle c_{i\alpha} c_{j\alpha}^\dagger \right\rangle, \quad (36)$$

Note that the Wilson loop becomes a two-point correlator. After gauge fixing the model loses the local gauge invariance, and the dimension of the Hilbert space is largely reduced. This gauge fixing process is illustrated in Fig. 2.
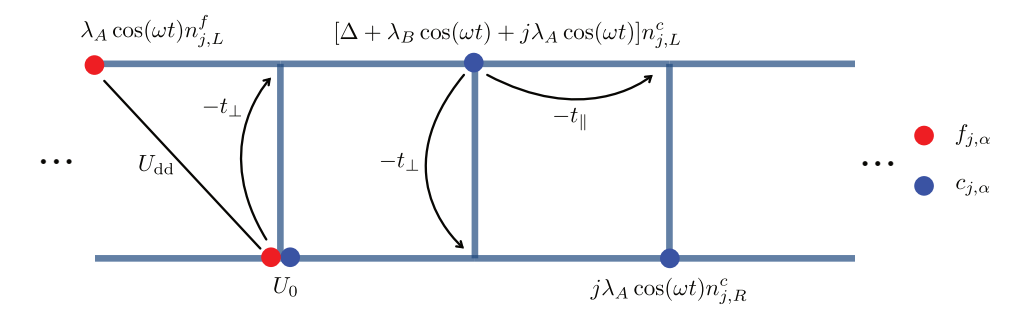
FIG. 3. Floquet engineering scheme. Red and blue points represents f and c fermions, respectively. The former can only hop along the rung direction (and each rung contains exactly one f femrion), while the latter can hop along both directions. There is an on-site interaction between them, and a dipole-dipole interaction between f fermions. Three time-dependent on-site potential $V_i(t)$, $i = 1, 2, 3$, are added. The first two are only applied to the left leg, while the last one is applied to both legs for the c fermion, with the amplitude increasing linearly from left to right.

IV. FLOQUET ENGINEERING OF THE HAMILTONIAN WITH FIXED GAUGE

Consider an optical lattice forming a ladder geometry, loaded with two types of fermions, c alkali atoms and f alkaline earth atoms with large magnetic dipole moment or polar molecules with large electric dipole moment, as shown in Fig. 3. The optical lattice is species dependent such that the c fermion can hop along both the leg and the rung directions, while the f fermions can only hop along the rung direction. Thus the hopping term of the Hamiltonian reads

$$H_0 = -t_\perp \sum_j (f_{jL}^\dagger f_{jR} + c_{jL}^\dagger c_{jR})$$
$$- t_\parallel \sum_{j\alpha} c_{j+1,\alpha}^\dagger c_{j\alpha} + \text{H.c.}, \quad (37)$$

where L (R) denotes the left (right) leg of the ladder. We further assume that the system is carefully prepared, and only one f fermion is loaded in each rung, i.e.,

$$n_{jL}^f + n_{jR}^f = 1, \quad \forall j. \quad (38)$$

There is an on-site interaction between two kinds of fermions, with strength U_0,

$$H_I = U_0 \sum_{j\alpha} n_{j\alpha}^f n_{j\alpha}^c. \quad (39)$$

A strong uniform magnetic field or an electric field is applied perpendicular to the plane of the ladder to polarized the f fermions. Thus the dipole moments of all f fermions are frozen to the perpendicular direction. As a result, the long range dipole-dipole interaction between the f fermions is

$$H_{\text{dd}} = \sum_{\alpha\beta,ij} U_{\text{dd}}\left(\mathbf{r}_{i\alpha} - \mathbf{r}_{j\beta}\right) n_{i\alpha}^f n_{j\beta}^f, \quad (40)$$

where $U_{\text{dd}}\left(\mathbf{r}\right) = C_{\text{dd}}/4\pi \left|\mathbf{r}\right|^3$. By tune the lattice spacing, one can ignore the dipole-dipole interaction beyond nearest neighboring rungs. Since there is only one f fermion on each rung, the spacing between f fermions on the nearest neighboring

rungs has twofold values, the lattice constant in the leg direction a and diagonal of the plaquette $\sqrt{a^2 + b^2}$, where b is the lattice constant in the rung direction. Then Eq. (40) can be simplified into

$$H_{\text{dd}} = U_1 \sum_{\alpha j} \left(n_{j\alpha}^f n_{j+1,\alpha}^f - n_{j\alpha}^f n_{j+1,\bar{\alpha}}^f \right) \quad (41)$$

where $U_1 = \left[U_{\text{dd}}\left(a\right) - U_{\text{dd}}\left(\sqrt{a^2 + b^2}\right)\right]/2$, and a constant is ignored.

We then modulate the on-site potential periodically, which consists of three parts, $V(t) = V_1(t) + V_2(t) + V_3(t)$, where

$$V_1(t) = \sum_j \lambda_A \cos(\omega t) n_{jL}^f, \quad (42a)$$

$$V_2(t) = \sum_j [\Delta + \lambda_B \cos(\omega t)] n_{jL}^c, \quad (42b)$$

$$V_3(t) = \sum_j j\lambda_A \cos(\omega t)(n_{jR}^c + n_{jL}^c). \quad (42c)$$

Namely, on the left leg only there are periodically driven on-site potential $V_{1,2}(t)$ for both types of fermions, with different amplitudes, $\lambda_{A,B}$, and a relative energy offset Δ. For the c fermion, there is an additional periodically driven grediant potential $V_3(t)$ along both legs. The full Hamiltonian is then given by $H = H_0 + H_I + H_{\text{dd}} + V(t)$. The energy offset and the driving frequency are turned such that

$$\omega = \Delta = U_0/2 \gg U_1, t_\perp, t_\parallel, \quad (43)$$

We now derive the time-independent, effective Hamiltonian of the system. Via a unitary transformation,

$$R(t) = e^{i \int_0^t d\tau [H_I + V(\tau)]}, \quad (44)$$

the fermion operator $b_{j\alpha}$, for $b = f$ or c, generally transforms in the following way,

$$R(t)b_{j\alpha}R^\dagger(t) = [(1 - n_{j\alpha}^{\bar{b}}) + n_{j\alpha}^{\bar{b}} e^{-i2\omega t}]e^{-i\theta_{j\alpha}^a(t)}b_{j\alpha}, \quad (45)$$

where $\bar{b} = f\ (c)$ if $b = c\ (f)$ and

$$\theta_{jL}^f(t) = \frac{\lambda_A}{\omega}\sin(\omega t), \tag{46}$$

$$\theta_{jR}^f(t) = 0, \tag{47}$$

$$\theta_{jL}^c(t) = \omega t + \frac{j\lambda_A + \lambda_B}{\omega}\sin(\omega t), \tag{48}$$

$$\theta_{jR}^c(t) = \frac{j\lambda_A}{\omega}\sin(\omega t). \tag{49}$$

I.e., the fermion oprerator acquires both a time-dependent operator factor and a numerical phase factor. The former, resulting from the interaction in Eq. (44), depends on the population of the other kind of fermion, while the latter can be viewed as a gauge transformation. Indeed, one trades off the time-dependent scalar potential (electric field) in Eq. (42) by a time-dependent vector potential, appearing as a phase due to the Peierls substitution. The full Hamiltonian in the rotating frame then becomes

$$H_R(t) \equiv R(t)H(t)R^\dagger(t) - R(t)i\partial_t R^\dagger(t) \tag{50}$$

$$= \{-t_\perp \sum_j [\hat{A}_j^f(t)e^{i\delta\theta_j^f(t)}f_{jL}^\dagger f_{jR}$$

$$+ \hat{A}_j^c(t)e^{i\delta\theta_j^c(t)}c_{jL}^\dagger c_{jR}]$$

$$- t_\parallel \sum_{j\alpha}[\hat{A}_j^\alpha(t)e^{i\delta\theta_j^\alpha}c_{j+1,\alpha}^\dagger c_{j\alpha}] + \text{H.c.}\} + H_{\text{dd}}, \tag{51}$$

where each hopping term contains an additional time-dependent operator, given respectively by

$$\hat{A}_j^f(t) = (1 - n_{jL}^c)(1 - n_{jR}^c) + n_{jL}^c n_{jR}^c$$

$$+ (1 - n_{jL}^c)n_{jR}^c e^{-i2\omega t} + n_{jL}^c(1 - n_{jR}^c)e^{i2\omega t}, \tag{52}$$

$$\hat{A}_j^c(t) = (1 - n_{jL}^f)n_{jR}^f e^{-i2\omega t} + (1 - n_{fR}^f)n_{jL}^f e^{i2\omega t}, \tag{53}$$

$$\hat{A}_j^\alpha(t) = \left(1 - n_{j+1,\alpha}^f\right)\left(1 - n_{j\alpha}^f\right)$$

$$+ n_{j+1,\alpha}^f n_{j\alpha}^f + (1 - n_{j+1,\alpha}^f)n_{j\alpha}^f e^{-i2\omega t}$$

$$+ n_{j+1,\alpha}^f(1 - n_{j\alpha}^f)e^{i2\omega t}, \tag{54}$$

where we have used Eq. (38) to simplify Eq. (53). The phase differences shown in Eq. (51) are

$$\delta\theta_j^f(t) = \theta_{jL}^f(t) - \theta_{jR}^f(t) = \frac{\lambda_A}{\omega}\sin(\omega t), \tag{55}$$

$$\delta\theta_j^c(t) = \theta_{jL}^c(t) - \theta_{jR}^c(t) = \omega t + \frac{\lambda_B}{\omega}\sin(\omega t), \tag{56}$$

$$\delta\theta_j^\alpha(t) = \theta_{j+1,\alpha}^c - \theta_{j\alpha}^c = \frac{\lambda_A}{\omega}\sin(\omega t), \quad \alpha = L, R. \tag{57}$$

Up to this point, everything is exact. Now consider the case with $\omega \gg t_\parallel, t_\perp$, which enables us to perform a high-frequency expansion on the rotated Hamiltonian Eq. (51). Using the Jacobi-Anger identity, $e^{iz\sin\phi} = \sum_{n=-\infty}^{\infty} J_n(z)e^{in\phi}$,

the effective Hamiltonian at the leading order becomes

$$H_{\text{eff}} \approx [-t_\perp \sum_j(\hat{B}_j^f f_{jL}^\dagger f_{jR} + \hat{B}_j^c c_{jL}^\dagger c_{jR})$$

$$- t_\parallel \sum_{j\alpha} \hat{B}_j^\alpha c_{j+1,\alpha}^\dagger c_{j\alpha} + \text{H.c.}]$$

$$+ U_1 \sum_j(n_{jL}^f - n_{jR}^f)(n_{j+1,L}^f - n_{j+1,R}^f), \tag{58}$$

where the operator associated with each hopping term now respectively becomes

$$\hat{B}_j^f = J_0\left(\frac{\lambda_A}{\omega}\right)[(1 - n_{jL}^c)(1 - n_{jR}^c) + n_{jL}^c n_{jR}^c]$$

$$+ J_2\left(\frac{\lambda_A}{\omega}\right)[(1 - n_{jL}^c)n_{jR}^c + n_{jL}^c(1 - n_{jR}^c)], \tag{59a}$$

$$\hat{B}_j^c = J_1\left(\frac{\lambda_B}{\omega}\right)(1 - n_{jL}^f)n_{jR}^f - J_3\left(\frac{\lambda_B}{\omega}\right)(1 - n_{fR}^f)n_{jL}^f, \tag{59b}$$

$$\hat{B}_j^\alpha = J_0\left(\frac{\lambda_A}{\omega}\right)\left[\left(1 - n_{j+1,\alpha}^f\right)\left(1 - n_{j\alpha}^f\right) + n_{j+1,\alpha}^f n_{j\alpha}^f\right]$$

$$+ J_2\left(\frac{\lambda_A}{\omega}\right)[(1 - n_{j+1,\alpha}^f)n_{j\alpha}^f + n_{j+1,\alpha}^f(1 - n_{j\alpha}^f)], \tag{59c}$$

where we have used the property of the Bessel function of the first kind that $J_{-m}(z) = (-1)^m J_m(z)$. Finally, setting

$$J_2\left(\frac{\lambda_A}{\omega}\right) = J_0\left(\frac{\lambda_A}{\omega}\right), \quad J_3\left(\frac{\lambda_B}{\omega}\right) = J_1\left(\frac{\lambda_B}{\omega}\right), \tag{60}$$

Eq. (59) is then simplified dramatically,

$$\hat{B}_j^f = \hat{B}_j^\alpha = J_0\left(\frac{\lambda_A}{\omega}\right), \tag{61}$$

$$\hat{B}_j^c = J_1\left(\frac{\lambda_B}{\omega}\right)(n_{jR}^f - n_{fL}^f). \tag{62}$$

Physically speaking, by tuning the lattice modulation amplitude λ_A, the hopping process of one fermions can become no longer sensitive to the population of the other kind, as schematically illustrated in Fig. 4(a). This mechanism works for both the f fermion, and the c fermions hopping along the legs. We further utilize the property that the Bessel function of the first kind satisfies $J_m(z) = -J_{-m}(z)$, for m odd, to effectively flips the sign of hopping strength for c fermions when hop along the rungs, depending on the population of the f fermion, as illustrated in Fig. 4(b). By finally defining the local spin operator

$$\sigma_j^z = n_{jL}^f - n_{jR}^f, \tag{63}$$

$$\sigma_j^x = f_{jL}^\dagger f_{jR} + f_{jR}^\dagger f_{jL}, \tag{64}$$

$$\sigma_j^y = -i(f_{jL}^\dagger f_{jR} - f_{jR}^\dagger f_{jL}), \tag{65}$$
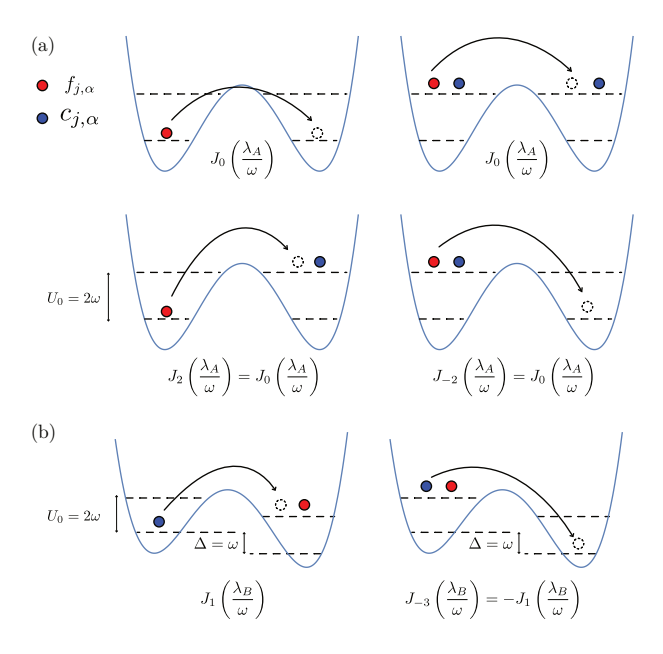
FIG. 4. The hopping process of fermions $f_{j,\alpha}$ in the double well can be understood in (a); while the hopping of fermions $c_{j,\alpha}$ in the transverse double well can be understood in (b). The hopping process of fermions $c_{j,\alpha}$ in the longitudinal direction has a similar mechanism as (a).

the effective Hamiltonian takes the following compact form:

$$
\begin{aligned}
H_{\text{eff}} = & -\tilde{t}_\parallel \sum_{j\alpha} \left(c_{j\alpha}^\dagger c_{j+1,\alpha} + \text{H.c.} \right) \\
& - \tilde{t}_\perp \sum_j \left(c_{jL}^\dagger \sigma_j^z c_{jR} + \text{H.c.} \right) \\
& - h \sum_j \sigma_j^x + U_1 \sum_j \sigma_j^z \sigma_{j+1}^z,
\end{aligned}
\tag{66}
$$

where

$$
\tilde{t}_\parallel = t_\parallel J_0 \left(\frac{\lambda_A}{\omega} \right),
\tag{67}
$$

$$
\tilde{t}_\perp = t_\perp J_1 \left(\frac{\lambda_B}{\omega} \right),
\tag{68}
$$

$$
h = t_\perp J_0 \left(\frac{\lambda_A}{\omega} \right).
\tag{69}
$$

Note that the long range dipole-dipole interaction maps to the Ising interaction between the spins on the rungs. This Hamiltonian is precisely the gauge-fixed Hamiltonian we discussed in the last section, Eq. (34). Hereafter, we will drop the tilde symbol for parameters used in Eq. (66) for simplicity.

This effective Hamiltonian has fermion charge U(1) symmetry, generated by $U_c(\phi) = e^{i\phi n}$, where $n = \sum_{j\alpha} n_{j\alpha}$ and $[n, H_{\text{eff}}] = 0$. There is another global U(1) symmetry generated by $R_x(\phi) = e^{i\phi S_x}$, where $S^x = \frac{1}{2} \sum_j \left(c_{jL}^\dagger c_{jR} + \text{H.c.} \right)$ and $[S^x, H_{\text{eff}}] = 0$. Moreover, Eq. (66) also has a discrete global $\mathbb{Z}_2$ symmetry generated by one of the following operators,

$$
Q_\alpha = \prod_j e^{i\pi n_{j\alpha}} \sigma_j^x, \quad \text{for} \quad \alpha = L, R.
\tag{70}
$$

These two operators are related by a global U(1) rotation, $I_L I_R = U_c(\pi)$. Also note that $Q_\alpha^2 = 1$, hence their eigenvalues are ± 1. Under this $\mathbb{Z}_2$ symmetry transformation, we have

$$
\sigma_j^z \to Q_\alpha \sigma_j^z Q_\alpha^{-1} = -\sigma_j^z, \quad \forall j.
\tag{71}
$$

Hence, a nonzero ground state expectation value of σ_j^z corresponds to spontaneously breaking this global $\mathbb{Z}_2$ symmetry. The system also has a particle-hole (PH) symmetry at half filling, namely, under the unitary PH transformation, $c_j \to (-1)^j c_j^\dagger$ and $c_j^\dagger \to (-1)^j c_j$, the Hamiltonian is invariant. Note this PH symmetry not only swaps particles and holes, i.e., $N_c \to 2N - N_c$, but also flips the sign of the global $\mathbb{Z}_2$ charge $Q_\alpha \to (-1)^N Q_\alpha$ if the total number of rungs N is odd.

V. ANALYTICAL RESULTS IN THE LIMITING CASES

In this section, we study two limiting cases of our effective Hamiltonian Eq. (66). It is found that, for the electric field strength h sufficiently small, the system is in the gapped phase with spontaneously broken global $\mathbb{Z}_2$ symmetry. In the large h limit, the system also remains charge gapped at half-filling.

A. The small h limit: Peierls instability

We start with the $h = U_1 = 0$ case, where quantum fluctuations of the Ising fields are turned off, hence all σ_i^z are conserved quantities and the full Hilbert space becomes a direct sum of different Ising spin configurations. In each sector, the model describes free fermions on a ladder, with the hopping strength along two legs being $t_\parallel$, and along rungs being $\pm t_{i,\perp}$, where the $\pm$ sign corresponds to the eigenvalue of σ_i^z. This Hamiltonian can be solved easily via exact diagonalization. And we find numerically that, at half filling, the lowest energy among all sectors corresponds to a Néel-type antiferromagnetic ordering for these Ising spins. This ground state spontaneously breaks the translational symmetry, and each plaquette contains a π flux, which resembles the dimerized lattice distortion that underlies the fermionic Peierls instability at half filling [58]. Adding a small positive U_1 does not modify this picture, since the spin-spin Ising interaction is also anti-ferromagnetic.

To elaborate on this analogy, and also to go to a finite but small $\mathbb{Z}_2$ electric field strength $h \ll t_{\parallel,\perp}$, we consider a Born-Oppenheimer-type approximation [59]. Namely, we assume that the fermions adapt instantaneously to the Ising spin background. Thus the latter provides an effective potential energy for the former, which in turn determines the ground-state spin configuration. This amounts to using the following variational
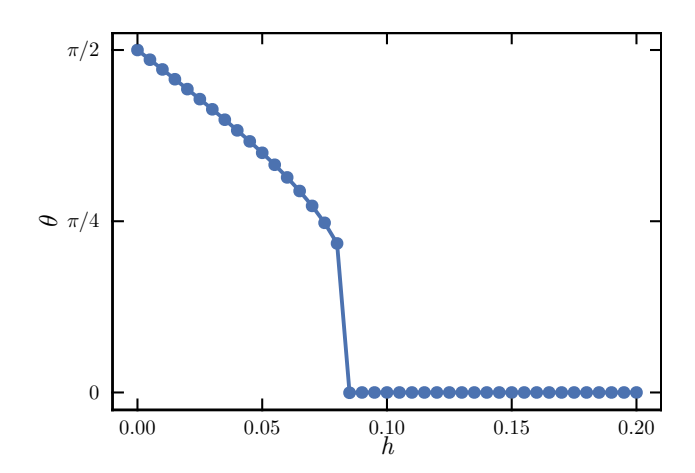
FIG. 5. Rotation angle θ as a function of transverse field h obtained by minimizing the ground state energy ϵ_{GS}, for fixed $t_\perp = 0.1$ and $U_1 = 0.2$.

wavefunction ansatz

$$|\Psi_{\mathrm{GS}}\rangle = \left|\psi_{\mathrm{GS}}^f\right\rangle \otimes e^{-i\sum_i \frac{\theta_i}{2}\sigma_i^y} |\uparrow\uparrow \cdots \uparrow\rangle_x, \qquad (72)$$

where $\left|\psi_{\mathrm{GS}}^f\right\rangle$ is the fermion wavefunction, say, in the local site Fock basis, and $|\uparrow\uparrow \cdots \uparrow\rangle_x$ means all spins pointing to the $+x$ direction. For fermions at half filling, the numerical result has showed the doubling of the unit cell for the ground state, we thus use a single variational angles $(\theta_{2i-1}, \theta_{2i}) = (\theta, -\theta)$ for the Ising spins due to reflection symmetry. Then the ground state energy can be written as an analytical function of θ, $t_\perp$, h and U_1 (we set $t_\parallel$ as the energy unit):

$$\epsilon_{\mathrm{GS}}(\theta) = 8\sqrt{4 + t_\perp^2 \sin^2\theta}\,\mathrm{E}\left(\frac{4}{4 + t_\perp^2 \sin^2\theta}\right)$$
$$- h\cos\theta - U_1 \sin^2\theta \qquad (73)$$

where $\mathrm{E}(x) := \int_0^{\pi/2} \sqrt{1 - x\sin^2\theta}\,d\theta$ is the complete elliptic integral of the second kind. One can then straightforwardly minimize this ground state energy for a fixed $t_\perp$, h and U_1 to find the optimal θ. In Fig. 5, we plot the numerical results for θ as a function of h obtained by minimizing the ground state energy ϵ_{GS} with fixed $t_\perp = 0.1$ and $U_1 = 0.2$. It shows that under this Born-Oppenheimer-type approximation, there is a first-order quantum phase transition between the symmetry-breaking antiferromagentic phase to the disordered paramagnetic phase.

Recall the Peierls instability of the SSH model [60], where the energy reduction of the fermions due to a gap opening is compensated by the increase of elastic energy of the lattice distortion [58]. Here, the $\mathbb{Z}_2$ electric field term, $-h\cos\theta$, plays the role of elastic energy. The central difference in this analogy is that while the one-dimensional fermion chain is always unstable towards a dimerization due to Peierls instability; here, for large h, the mechanism does not work. This is due to the fact that our assumption, the Born-Oppenheimer-type argument, fails, i.e., Eq. (72) becomes inappropriate.

B. The large h limit: repulsive Hubbard model

In the infinite h limit, the system becomes two decoupled fermion chains, which is gapless. A large but finite h introduces coupling between these two chains. To examine the fate of this infinite-h gapless phase under such perturbations, in the following, we will derive the effective Hamiltonian for Eq. (66) in the large h limit, then phases of the resulting Hamiltonian is discussed. Since U_1 is small in our experimental scheme, in the following discussion we will focus on the case with $U_1 = 0$, and it is expect that the conclusion holds for a small nonzero U_1.

We start by writing the original Hamiltonian Eq. (66) with $U_1 = 0$ as $H = hH_0 + H_1 + V$, where

$$H_0 = -\sum_i \sigma_i^x, \qquad (74)$$

$$H_1 = -t_\parallel \sum_{\langle ij\rangle,\tau} \left(c_{i\tau}^\dagger c_{j\tau} + \mathrm{H.c.}\right), \qquad (75)$$

$$V = -t_\perp \sum_i \left(c_{i,L}^\dagger \sigma_i^z c_{i,R} + \mathrm{H.c.}\right). \qquad (76)$$

Upon a canonical and unitary transformation, $|\psi'\rangle = e^{iS}|\psi\rangle$, where S is Hermitian and time-independent, it becomes (using the Baker-Campbell-Hausdorff formula),

$$\tilde{H} = e^{iS}He^{-iS} = H + i[S, H] + \frac{i^2}{2!}[S, [S, H]] + \cdots. \quad (77)$$

We write the operator S as a series expansion in h^{-1},

$$S = S^{(1)}h^{-1} + S^{(2)}h^{-2} + \cdots = \sum_{l=1}^\infty S^{(l)}h^{-l}. \qquad (78)$$

Up to the zeroth order in h^{-1}, Eq. (77) reads

$$H' = hH_0 + H_1 + V + i[S^{(1)}, H_0] + \mathcal{O}(h^{-1}). \qquad (79)$$

By choosing $S^{(1)} = \frac{t_\perp}{2}\sum_i \left(\sigma_i^y c_{iL}^\dagger c_{iR} + \mathrm{H.c.}\right)$, we have $V + i[S^{(1)}, H_0] = 0$. And the effective Hamiltonian Eq. (79) after the projection, $PH'P$, where P projects to the low-energy subspace with all spins pointing to the $+\hat{x}$ direction, becomes (omitting the constant)

$$\tilde{H}^{(1)} = -t_\parallel \sum_{\langle ij\rangle\tau} \left(c_{i\tau}^\dagger c_{j\tau} + \mathrm{H.c.}\right) + \mathcal{O}(h^{-1}), \qquad (80)$$

which is just two free fermion chain, as expected. Up to the first order in h^{-1}, Eq. (77) becomes

$$\begin{aligned} H' = &\, hH_0 + H_1 \\ &+ (i[S^{(1)}, H_1] + i[S^{(1)}, V] + i[S^{(2)}, H_0])h^{-1} \\ &+ \mathcal{O}(h^{-2}). \end{aligned} \qquad (81)$$

where the first commutator reads

$$i[S^{(1)}, H_1] = -\frac{it_\perp t_\parallel}{2}\sum_{\langle ij\rangle\tau}(\sigma_i^y - \sigma_j^y)(c_{i\tau}^\dagger c_{j\bar\tau} - c_{j\tau}^\dagger c_{i\bar\tau}), \quad (82)$$
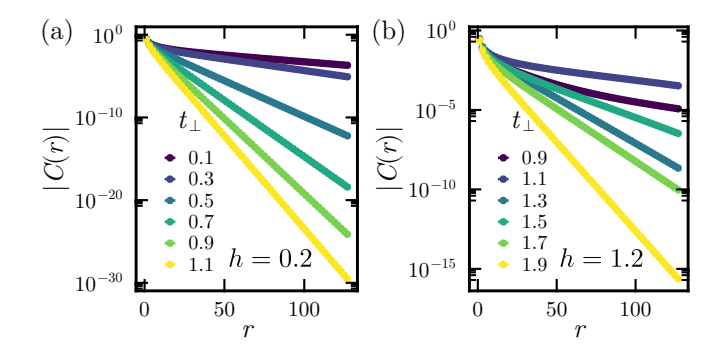
FIG. 6. Behavior of the gauge-invariant single-particle correlator of fermion matter, defined in Eq. (86), for (a) $h = 0.2$ and (b) $h = 1.2$. $t_\parallel = 1$ is set as the energy unit, and $U_1 = 0.1$.

FIG. 7. Behavior of the modified Wilson loop $\tilde{W}(r)$, Eq. (87), for various h with $t_\perp = t_\parallel = 1$ and $U_1 = 0.1$.

with $\bar{\tau} = L\ (R)$ if $\tau = R\ (L)$. The second one is found to be $i[S^{(1)}, V] = t_\perp^2 \sum_i \sigma_i^x (2n_{iL} n_{iR} - n_i)$, with $n_i = n_{iL} + n_{iR}$. By choosing $S^{(2)}$ to eliminate the off-diagonal terms in the σ^x basis, namely, demanding that $i[S^{(1)}, H_1] + i[S^{(2)}, H_0] \overset{!}{=} 0$, we then have

$$S^{(2)} = -\frac{it_\perp t_\parallel}{4} \sum_{\langle ij \rangle \tau} (\sigma_i^z - \sigma_j^z)(c_{i\tau}^\dagger c_{j\bar{\tau}} - c_{j\tau}^\dagger c_{i\bar{\tau}}). \quad (83)$$

And Eq. (81) becomes (with constant terms omitted)

$$\tilde{H}^{(2)} = -t_\parallel \sum_{\langle ij \rangle \tau} \left(c_{i\tau}^\dagger c_{j\tau} + \text{H.c.} \right) + \frac{2t_\perp^2}{h} \sum_i \sigma_i^x n_{iL} n_{iR} + \mathcal{O}(h^{-2}). \quad (84)$$

In the large h limit, spins are polarized and are hard to fluctuate. Thus, one can replace σ_i^x by its expectation value, $\sigma_i^x \approx \langle \sigma_i^x \rangle \approx 1$. This replacement is equivalent to projecting the Hamiltonian into the low-energy manifold. Then we obtain

$$\tilde{H}^{(2)} = -t_\parallel \sum_{\langle ij \rangle \tau} \left(c_{i\tau}^\dagger c_{j\tau} + \text{H.c.} \right) + \frac{2t_\perp^2}{h} \sum_i n_{iL} n_{iR} + \mathcal{O}(h^{-2}). \quad (85)$$

Note that this low energy effective Hamiltonian is equivalent to the one-dimensional Fermi Hubbard model with the repulsive interaction strength $U = 2t_\perp^2/h$, and hopping strength $t = t_\parallel$. The leg index $\tau = L, R$, plays the role of spin index.

The quantum phase diagram of the 1D repulsive Fermi Hubbard model as a function of U/t is well-known. For a given commensurate filling and increasing U/t, there is a quantum phase transition from the Luttinger liquid (metallic) phase to the Mott insulator phase of the Kosterlize-Thouless type. For half-filling, the transition point is at $U/t = 0$ [61]. That means the system will stay in the Mott phase at any finite on-site interaction strength. Combining with the analysis obtained from the small h limit, we conclude that the charge gap should always be open for the half-filling case at arbitrary finite h
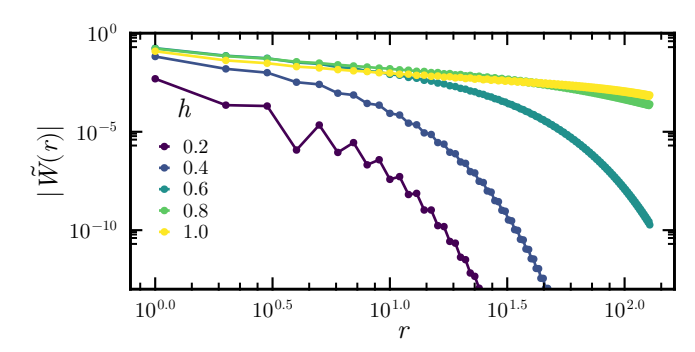
VI. NUMERICAL RESULTS: A DMRG STUDY

We now present the numerical results. We use the density matrix renormalization group algorithm [62] based on matrix product states [63] via the ITensor Library [64], to study the full phase diagram of the gauge-fixed model Eq. (66) at half filling. We emphasize that, behaviors of various gauge invariant quantities of the gauge-invariant Hamiltonian Eq. (21) can be examined from this gauge-fixed one. In the following simulations, $t_\parallel$ is fixed to be the energy unit, and we fix $U_1 = 0.1$. We choose the open boundary conditions with total rungs of ladder to be $L = 256$. The fermion number U(1) symmetry is used, with maximal bond dimension $D = 256$ and truncation error $\lesssim 10^{-6}$.

A. Fermion matter sector

We start with the fermion matter sector. First of all, in the half-filling case, it is found that the (gauge-invariant) charge density distribution is always uniform, with the corresponding density-density correlator always decaying exponentially. We then turn to the gauge-invariant single-particle correlator, defined in Eq. (26), which explicitly reads

$$C_{LL}(r) = \left\langle c_{i,L} \left(\prod_{j=i}^{i+r-1} \sigma_{jL}^z \right) c_{i+r,L}^\dagger \right\rangle$$

$$\xrightarrow{\text{gauge fixing}} \left\langle c_{i,L} c_{i+r,L}^\dagger \right\rangle. \quad (86)$$

The behavior of this quantity for different $t_\perp$ is shown in Fig. 6, one always finds an exponential decay, which is consistent with our theoretical analysis given in Sec. (V). Namely, the charge gap remains open for all h.

B. Ising gauge sector

One of the most important gauge-invariant observables in Ising gauge sector is the Wilson loop [65]. In its original context, the confinement-deconfinement transition can be defined by the area-law or perimeter-law decay of this quantity
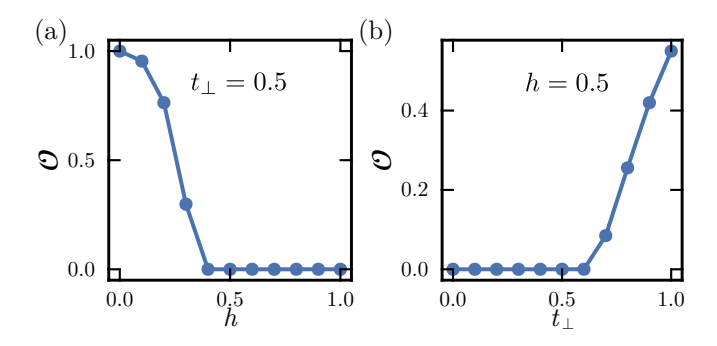
FIG. 8. Behavior of the order parameter $\mathcal{O}$, Eq. (88), as a function of (a) h with fixed $t_\perp = 0.5$ and (b) $t_\perp$ with fixed $h = 0.5$. $t_\parallel = 1$ is set as the energy unit, and $U_1 = 0.1$.

for a sufficiently large loop [66]. For a ladder geometry, it is defined in Eq. (25). After the gauge-fixing process, it reduces to a two-point correlator, Eq. (35). To clearly reveal its spatial dependence, we further consider its connected version, namely, the modified Wilson loop defined by

$$\tilde{W}(r) \equiv \left\langle \sigma_i^z \sigma_{i+r}^z \right\rangle_c$$
$$= \left\langle \sigma_i^z \sigma_{i+r}^z \right\rangle - \left\langle \sigma_i^z \right\rangle \left\langle \sigma_{i+r}^z \right\rangle. \quad (87)$$

In Fig 7, for fixed $t_\parallel = t_\perp = 1$ and $U_1 = 0.1$, we find that it exhibits an exponential decay for small h, and an power-law decay for large h, reminiscent of a strong area-law decay and weak perimeter-law decay in the original LGT, respectively.

C. Global $\mathbb{Z}_2$ symmetry breaking and full phase diagram

The effective Hamiltonian Eq. (66) has a global $\mathbb{Z}_2$ symmetry generated by Eq. (70). As discussed in Sec. V A, a Peierls instability mechanism will lead to a Néel-type ordering along spin-z direction for small h. Thus this symmetry is spontaneously broken there. By increasing h, these Ising spins will tend to aligned along spin-x direction. It is therefore expected that there is a order-disorder phase transition, in analog to the antiferromagnetic transverse field Ising chain. To identify the phase transition point explicitly, we use the order parameter defined by

$$\mathcal{O} = \frac{1}{N} \sum_i (-1)^i \left\langle \sigma_i^z \right\rangle. \quad (88)$$

In Fig. 8, this order parameter is plotted as a function of h with fixed $t_\perp = 0.5$, and as a function of $t_\perp$ with fixed $h = 0.5$. It is found that a sufficiently large h will kill the symmetry-breaking phase, while a sufficiently large $t_\perp$ will induce this symmetry-breaking phase. We then present the full phase diagram in Fig. 9(a). There are basically two phases, for large $t_\perp$ and small h, the system is in the antiferromagnetic (AFM) phase, while for h large and $t_\perp$ small, the system is in the paramagnetic phase (PM). In the AFM phase, the modified Wilson loop decays exponentially, which is a confinement-like phase, while in the PM phase it decays algebraically, which
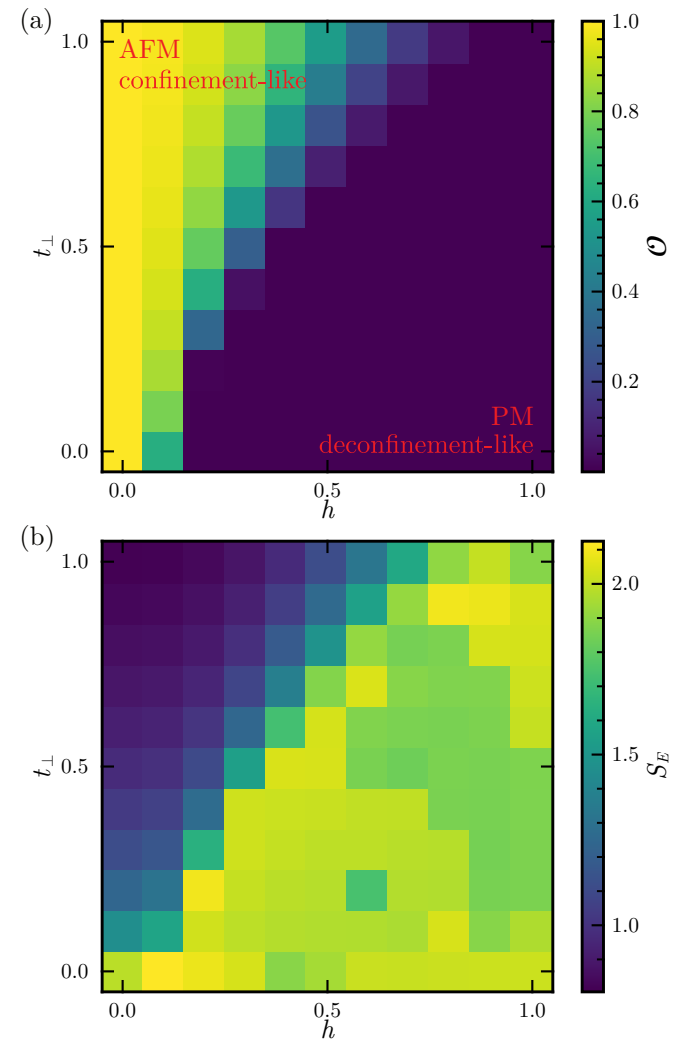

FIG. 9. (a) Contour plot of the order parameter $\mathcal{O}$. (b) Contour plot of the entanglement entropy S_E measured at the central site. The other parameters: $t_\parallel = 1$ and $U_1 = 0.1$.

is a deconfinement-like phase. Note that in both phases, the gauge-invariant single-particle correlator always decay exponentially. We also present contour plot of entanglement entropy measured at the central site in Fig. 9(b). It is found that the system is more entangled in the PM phase than the AFM phase. The phase transition boundary is also evident from this plot.

VII. SUMMARY AND OUTLOOK

In this work, we propose to quantum simulate LGT with gauge fixing. In particular, we firstly explain the concept of gauge fixing on the Hamiltonian level. We show that the matrix elements of the Hamiltonian of a LGT before and after gauge fixing are identical, as well as the matrix elements of the gauge invariant observable. Thus by quantum simulation LGTs with fixed gauge, one can acquire the full information

about the unfixed original models. Usually, the gauge fixed model is much simpler and easy to implement in experiments. Then we consider the simplest LGT, namely the Ising LGT, and discuss in details on how to fix the gauge for this model on a ladder geometry. After gauge fixing, it becomes a model describing fermions hopping on a ladder subject to a fluctuating dynamical flux. We then provide a Floquet engineering scheme to simulate the corresponding gauge-fixed Hamiltonian. Lastly, we study this gauge-fixed Hamiltonian in the limiting cases and use DMRG to investigate various gauge-invariant correlators and many-body phase diagram. There are basically two phases identified, one is the global $\mathbb{Z}_2$ symmetry breaking phase, i.e., the antiferromagnetic phase, where the modified Wilson loop operator decays exponentially, reminiscent of a strong area-law decay and confinement in the unfixed model. The other is the paramagnetic phase where the modified Wilson loop operator decays algebraically, and resembles a weak perimeter-law decay and deconfinement in the unfixed model.

In the future, it is interesting to consider LGT with other more complicated gauge symmetry group like U(1) or SU(2). It is expected that the gauge-fixed Hamiltonian for these models should be much simpler than the original ones for both quantum simulations and numerical calculations. We leave it for future studies to consider these more sophisticated cases.

[1] M. Creutz, *Quarks, Gluons and Lattices* (Cambridge University Press, 1983).

[2] I. Montvay, I. Montvay, and G. Münster, *Quantum fields on a lattice*, Cambridge monographs on mathematical physics (Cambridge University Press, Cambridge, 1997).

[3] H. J. Rothe, *Lattice Gauge Theories: An Introduction*, World Scientific Lecture Notes In Physics No. v.82 (World Scientific Publishing Company, Singapore, 2012).

[4] K. G. Wilson, Confinement of quarks, Phys. Rev. D **10**, 2445 (1974).

[5] C. Broholm, R. J. Cava, S. A. Kivelson, D. G. Nocera, M. R. Norman, and T. Senthil, Quantum spin liquids, Science **367**, eaay0668 (2020).

[6] P. A. Lee, N. Nagaosa, and X.-G. Wen, Doping a Mott insulator: Physics of high-temperature superconductivity, Rev. Mod. Phys. **78**, 17 (2006).

[7] U. Wiese, Ultracold quantum gases and lattice systems: quantum simulation of lattice gauge theories, Annalen der Physik **525**, 777 (2013).

[8] Z.-Y. Zhou, G.-X. Su, J. C. Halimeh, R. Ott, H. Sun, P. Hauke, B. Yang, Z.-S. Yuan, J. Berges, and J.-W. Pan, Thermalization dynamics of a gauge theory on a quantum simulator, Science **377**, 311 (2022).

[9] J. Mildenberger, W. Mruczkiewicz, J. C. Halimeh, Z. Jiang, and P. Hauke, Probing confinement in a $\mathbb{Z}_2$ lattice gauge theory on a quantum computer, arXiv:2203.08905 [quant-ph].

[10] H.-Y. Wang, W.-Y. Zhang, Z. Yao, Y. Liu, Z.-H. Zhu, Y.-G. Zheng, X.-K. Wang, H. Zhai, Z.-S. Yuan, and J.-W. Pan, Interrelated thermalization and quantum criticality in a lattice gauge simulator, Phys. Rev. Lett. **131**, 050401 (2023).

[11] W.-Y. Zhang, Y. Liu, Y. Cheng, M.-G. He, H.-Y. Wang, T.-Y. Wang, Z.-H. Zhu, G.-X. Su, Z.-Y. Zhou, Y.-G. Zheng, H. Sun, B. Yang, P. Hauke, W. Zheng, J. C. Halimeh, Z.-S. Yuan, and J.-W. Pan, Observation of microscopic confinement dynamics by a tunable topological θ-angle, arXiv:2306.11794 [cond-mat.quant-gas].

[12] E. A. Martinez, C. A. Muschik, P. Schindler, D. Nigg, A. Erhard, M. Heyl, P. Hauke, M. Dalmonte, T. Monz, P. Zoller, and R. Blatt, Real-time dynamics of lattice gauge theories with a few-qubit quantum computer, Nature **534**, 516 (2016).

[13] Z. Davoudi, M. Hafezi, C. Monroe, G. Pagano, A. Seif, and A. Shaw, Towards analog quantum simulations of lattice gauge theories with trapped ions, Phys. Rev. Res. **2**, 023015 (2020).

[14] F. M. Surace, P. P. Mazza, G. Giudici, A. Lerose, A. Gambassi, and M. Dalmonte, Lattice gauge theories and string dynamics in Rydberg atom quantum simulators, Phys. Rev. X **10**, 021041 (2020).

[15] Y. Cheng and H. Zhai, Emergent gauge theory in Rydberg atom arrays, arXiv:2401.07708 [cond-mat.quant-gas].

[16] T. Byrnes and Y. Yamamoto, Simulating lattice gauge theories on a quantum computer, Phys. Rev. A **73**, 022328 (2006).

[17] C. Muschik, M. Heyl, E. Martinez, T. Monz, P. Schindler, B. Vogell, M. Dalmonte, P. Hauke, R. Blatt, and P. Zoller, U(1) Wilson lattice gauge theories in digital quantum simulators, New Journal of Physics **19**, 103020 (2017).

[18] E. Zohar, A. Farace, B. Reznik, and J. I. Cirac, Digital lattice gauge theories, Phys. Rev. A **95**, 023604 (2017).

[19] J. Bender, E. Zohar, A. Farace, and J. I. Cirac, Digital quantum simulation of lattice gauge theories in three spatial dimensions, New Journal of Physics **20**, 093001 (2018).

[20] N. Klco, E. F. Dumitrescu, A. J. McCaskey, T. D. Morris, R. C. Pooser, M. Sanz, E. Solano, P. Lougovski, and M. J. Savage, Quantum-classical computation of Schwinger model dynamics using quantum computers, Phys. Rev. A **98**, 032331 (2018).

[21] N. Klco, M. J. Savage, and J. R. Stryker, Su(2) non-Abelian gauge field theory in one dimension on digital quantum computers, Phys. Rev. D **101**, 074512 (2020).

[22] S. V. Mathis, G. Mazzola, and I. Tavernelli, Toward scalable simulations of lattice gauge theories on quantum computers, Phys. Rev. D **102**, 094501 (2020).

[23] L. Tagliacozzo, A. Celi, P. Orland, M. W. Mitchell, and M. Lewenstein, Simulation of non-Abelian gauge theories with optical lattices, Nature Communications **4**, 10.1038/ncomms3615 (2013).

[24] E. Zohar, J. I. Cirac, and B. Reznik, Quantum simulations of lattice gauge theories using ultracold atoms in optical lattices, Reports on Progress in Physics **79**, 014401 (2015).

[25] F. F. Assaad and T. Grover, Simple fermionic model of deconfined phases and phase transitions, Phys. Rev. X **6**, 041049 (2016).

[26] D. González-Cuadra, E. Zohar, and J. I. Cirac, Quantum simulation of the Abelian-Higgs lattice gauge theory with ultracold atoms, New Journal of Physics **19**, 063038 (2017).

[27] A. Smith, J. Knolle, D. L. Kovrizhin, and R. Moessner, Disorder-free localization, Phys. Rev. Lett. **118**, 266601 (2017).

[28] M. Brenes, M. Dalmonte, M. Heyl, and A. Scardicchio, Many-body localization dynamics from gauge invariance, Phys. Rev. Lett. **120**, 030601 (2018).

[29] A. Smith, J. Knolle, R. Moessner, and D. L. Kovrizhin, Dynamical localization in $\mathbb{Z}_2$ lattice gauge theories, Phys. Rev. B **97**, 245137 (2018).

[30] T. V. Zache, F. Hebenstreit, F. Jendrzejewski, M. K. Oberthaler, J. Berges, and P. Hauke, Quantum simulation of lattice gauge theories using Wilson fermions, Quantum Science and Technology **3**, 034010 (2018).

[31] Z. Yao, C. Liu, P. Zhang, and H. Zhai, Many-body localization from dynamical gauge fields, Phys. Rev. B **102**, 104302 (2020).

[32] W. Zheng and P. Zhang, Floquet engineering of a dynamical $\mathbb{Z}_2$ lattice gauge field with ultracold atoms, arXiv:2011.01500 [cond-mat.quant-gas].

[33] J. C. Halimeh and P. Hauke, Reliability of lattice gauge theories, Phys. Rev. Lett. **125**, 030503 (2020).

[34] M. Van Damme, J. C. Halimeh, and P. Hauke, Gauge-symmetry violation quantum phase transition in lattice gauge theories, arXiv:2010.07338 [cond-mat.quant-gas].

[35] J. C. Halimeh, V. Kasper, and P. Hauke, Fate of lattice gauge theories under decoherence (), arXiv:2009.07848 [cond-mat.quant-gas].

[36] J. C. Halimeh, H. Lang, J. Mildenberger, Z. Jiang, and P. Hauke, Gauge-symmetry protection using single-body terms, PRX Quantum **2**, 040311 (2021).

[37] E. Zohar, Quantum simulation of lattice gauge theories in more than one space dimension—requirements, challenges and methods, Philosophical Transactions of the Royal Society A: Mathematical, Physical and Engineering Sciences **380**, 10.1098/rsta.2021.0069 (2021).

[38] Y. Cheng, S. Liu, W. Zheng, P. Zhang, and H. Zhai, Tunable confinement-deconfinement transition in an ultracold-atom quantum simulator, PRX Quantum **3**, 040317 (2022).

[39] C. Gao, J. Liu, M. Chang, H. Pu, and L. Chen, Synthetic u(1) gauge invariance in a spin-1 bose gas, Phys. Rev. Res. **4**, L042018 (2022).

[40] J. C. Halimeh, L. Homeier, C. Schweizer, M. Aidelsburger, P. Hauke, and F. Grusdt, Stabilizing lattice gauge theories through simplified local pseudogenerators, Phys. Rev. Res. **4**, 033120 (2022).

[41] J. C. Halimeh, L. Homeier, H. Zhao, A. Bohrdt, F. Grusdt, P. Hauke, and J. Knolle, Enhancing disorder-free localization through dynamically emergent local symmetries, PRX Quantum **3**, 020345 (2022).

[42] C. Gao, Z. Tang, F. Zhu, Y. Zhang, H. Pu, and L. Chen, Nonthermal dynamics in a spin-$\frac{1}{2}$ lattice schwinger model, Phys. Rev. B **107**, 104302 (2023).

[43] J. Osborne, I. P. McCulloch, and J. C. Halimeh, Disorder-free localization in $2 + 1$D lattice gauge theories with dynamical matter, arXiv:2301.07720 [cond-mat.quant-gas].

[44] L. Homeier, A. Bohrdt, S. Linsel, E. Demler, J. C. Halimeh, and F. Grusdt, Realistic scheme for quantum simulation of $\mathbb{Z}_2$ lattice gauge theories with dynamical matter in (2+1)D, Communications Physics **6**, 10.1038/s42005-023-01237-6 (2023).

[45] J. C. Halimeh, M. Aidelsburger, F. Grusdt, P. Hauke, and B. Yang, Cold-atom quantum simulators of gauge theories (), arXiv:2310.12201 [cond-mat.quant-gas].

[46] J. C. Halimeh, L. Barbiero, P. Hauke, F. Grusdt, and A. Bohrdt, Robust quantum many-body scars in lattice gauge theories, Quantum **7**, 1004 (2023).

[47] M. Van Damme, H. Lang, P. Hauke, and J. C. Halimeh, Reliability of lattice gauge theories in the thermodynamic limit, Phys. Rev. B **107**, 035153 (2023).

[48] M. c. v. Kebrič, J. C. Halimeh, U. Schollwöck, and F. Grusdt, Confinement in $(1 + 1)$-dimensional $\mathbb{Z}_2$ lattice gauge theories at finite temperature, Phys. Rev. B **109**, 245110 (2024).

[49] G.-X. Su, J. Osborne, and J. C. Halimeh, A cold-atom particle collider, arXiv:2401.05489 [cond-mat.quant-gas].

[50] H.-Y. Qi and W. Zheng, Gauge violation spectroscopy of synthetic gauge theories, Phys. Rev. Res. **6**, 013047 (2024).

[51] Z. Tang, F. Zhu, Y.-F. Luo, W. Zheng, and L. Chen, Partial confinement in a quantum-link simulator, arXiv:2404.18095 [cond-mat.quant-gas].

[52] C. Schweizer, F. Grusdt, M. Berngruber, L. Barbiero, E. Demler, N. Goldman, I. Bloch, and M. Aidelsburger, Floquet approach to $\mathbb{Z}_2$ lattice gauge theories with ultracold atoms in optical lattices, Nature Physics **15**, 1168 (2019).

[53] B. Yang, H. Sun, R. Ott, H.-Y. Wang, T. V. Zache, J. C. Halimeh, Z.-S. Yuan, P. Hauke, and J.-W. Pan, Observation of gauge invariance in a 71-site Bose–Hubbard quantum simulator, Nature **587**, 392 (2020).

[54] A. Mil, T. V. Zache, A. Hegde, A. Xia, R. P. Bhatt, M. K. Oberthaler, P. Hauke, J. Berges, and F. Jendrzejewski, A scalable realization of local U(1) gauge invariance in cold atomic mixtures, Science **367**, 1128 (2020).

[55] M. Creutz, L. Jacobs, and C. Rebbi, Monte Carlo computations in lattice gauge theories, Phys. Rep. **95**, 201 (1983).

[56] L. Faddeev and V. Popov, Feynman diagrams for the Yang-Mills field, Physics Letters B **25**, 29 (1967).

[57] B. S. DeWitt, Quantum theory of gravity. II. the manifestly covariant theory, Phys. Rev. **162**, 1195 (1967).

[58] R. E. Peierls, *Quantum Theory of Solids* (Oxford University Press, 2001).

[59] D. González-Cuadra, A. Dauphin, P. R. Grzybowski, P. Wójcik, M. Lewenstein, and A. Bermudez, Symmetry-breaking topological insulators in the $\mathbb{Z}_2$ Bose-Hubbard model, Phys. Rev. B **99**, 045139 (2019).

[60] W. P. Su, J. R. Schrieffer, and A. J. Heeger, Solitons in Polyacetylene, Phys. Rev. Lett. **42**, 1698 (1979).

[61] T. Giamarchi, Mott transition in one dimension, Phys. B: Condens. Matter **230-232**, 975 (1997).

[62] S. R. White, Density matrix formulation for quantum renormalization groups, Phys. Rev. Lett. **69**, 2863 (1992).

[63] U. Schollwöck, The density-matrix renormalization group in the age of matrix product states, Annals of Physics **326**, 96 (2011).

[64] M. Fishman, S. White, and E. Stoudenmire, The ITensor software library for tensor network calculations, SciPost Physics Codebases 10.21468/scipostphyscodeb.4 (2022).

[65] J. B. Kogut, An introduction to lattice gauge theory and spin systems, Rev. Mod. Phys. **51**, 659 (1979).

[66] R. Shankar, *Quantum Field Theory and Condensed Matter* (Cambridge University Press, 2017).